Classification: BIOLOGICAL SCIENCES: Biochemsitry

Structure of bacterial cellulose synthase subunit D octamer with four inner passageways

Song-Qing Hu[a,1,2], Yong-Gui Gao[a,1,2], Kenji Tajima[b,1], Naoki Sunagawa[b], Yong Zhou[a], Shin Kawano[b,2], Takaaki Fujiwara[a], Takanori Yoda[b], Daisuke Shimura[b], Yasuharu Satoh[b], Masanobu Munekata[b], Isao Tanaka[a], and Min Yao[a,3]

[a]Faculty of Advanced Life Science, Hokkaido University, Sapporo 060-0810, Japan; [b]Division of Biotechnology and Macromolecular Chemistry, Graduate School of Engineering, Hokkaido University, Sapporo 060-8628, Japan.

[1]These authors contributed equally to this work.

[2]Current address: College of Light Industry and Food Sciences, South China University of Technology, Guangzhou 510640, China for SongQing Hu; MRC Laboratory of Molecular Biology, Hills Road, Cambridge CB2 0QH, UK for Yong-Gui Gao; Database Center for Life Science, Research Organization of Information and Systems, 2-11-16 Yayoi, Bunkyo-ku, Tokyo 113-0032, Japan for Shin Kawano

[3]Corresponding author: E-mail: yao@castor.sci.hokudai.ac.jp, Telephone: +81 11 706 4481, Fax: +81 11 706 4481

Number of text pages/figures/table: 23/3/0

Abbreviations: bacterial cellulose (BC); terminal complex (TC); cellopentaose (CPT); multiple anomalous diffraction (MAD); root mean square deviation (RMSD); sub-elementary fibril (SEF); scanning electron microscope (SEM); uridine diphosphate glucose (UDP-Glc)

Data deposition footnote: The atomic coordinates have been deposited in the Protein Databank (www.pdb.org) with code 3AJ1 (N_AxCeSD), 3AJ2 (C_AxCeSD), and 3A8E (C_AxCeSD-CPT)

Abstract

The cellulose synthesizing terminal complex consisting of subunits A, B, C, and D in *Acetobacter xylinum* spans the outer and inner cell membranes to synthesize and extrude glucan chains, which are assembled into sub-elementary fibrils and further into a ribbon. We determined the structures of subunit D (AxCeSD/AxBcsD) with both N- and C-terminal His_6-tag, and in complex with cellopentaose. The structure of AxCeSD shows an exquisite cylinder shape (height: ~65 Å, outer diameter: ~90 Å, and inner diameter: ~25 Å) with a right-hand twisted dimer interface on the cylinder-wall, formed by octamer as a functional unit. All N-termini of the octamer are positioned inside the AxCeSD cylinder and create four passageways. The location of cellopentaoses in the complex structure suggests that four glucan chains are extruded individually through their own passageway along the dimer interface in a twisted manner. The complex structure also shows that the N-terminal loop, especially residue Lys6, seems to be important for cellulose production, as confirmed by *in vivo* assay using mutant cells with *axcesD* gene disruption and N-terminus truncation. Taking all results together, a model of the bacterial terminal complex is discussed.

Keywords: crystal structure, cellulose synthasis

\body

Introduction

Cellulose is a linear homopolymer of D-glucopyranose linked by β-1,4-glycosidic bonds. It is an abundant polysaccharide in nature, and accounts for over half of the total organic carbon in the earth's biosphere. Cellulose is produced by many different organisms, including vascular plants, algae, some bacteria, and even some animals (1-5). Among these, bacterial cellulose (BC) produced by gram-negative obligate aerobe *Acetobacter xylinum* (*A. xylinum* = *Gluconacetobacter xylinus*), has exceptional physicochemical properties, such as ultrafine reticulated structure, high crystallinity, high tensile strength, high hydrophilicity, moldability during formation, and biocompatibility, although its chemical structure is similar to those of cellulose produced by plants and algae (2, 6, 7). These remarkable characteristics are of interest for the development and manufacture of a wide range of commercial materials, such as food matrix, dietary fiber, acoustic membranes, special biomaterials (8, 9), optically transparent material additives (10), and electronic displays (11). Several techniques and the optimum culture conditions are used for BC production. However, both the scale and cost of production still impede a wide range of applications of BC (7, 12, 13). The elucidation of cellulose biosynthesis by *A. xylinum* is indispensable for the efficient cellulose production and industrial applications.

A. xylinum has been used for many years as a model organism to study cellulose biosynthesis (14-16). In *A. xylinum*, the cellulose synthesizing terminal complexes (referred to TCs) are arrayed in a linear row along the longitudinal axis of the cell (17, 18). One TC consists of at least four subunits, AxCeSA (cellulose synthase subunit A), AxCeSB (subunit B), AxCeSC (subunit C), and AxCeSD (subunit D), which are encoded by three (*axcesAB*,

axcesC, and *axcesD*) or four (*axcesA*, *axcesB*, *axcesC*, and *axcesD*) genes that form a cellulose synthase operon (*axces*) (19-23). There has been a great deal of research to determine the functions of these subunits. AxCeSA and AxCeSB are responsible for catalyzing and regulating glucan chain polymerization, respectively (21). AxCeSC and AxCeSD are believed to play roles in glucan chain extrusion and crystallization, which are thought to be rate-limiting steps during the coupled processes of polymerization and crystallization in cellulose assembly (16, 21, 24). The sites of cellulose synthesis on the cell surface were observed as crater-like ring wall structures ~150 Å in diameter with a central hole or deepening of ~35 Å (circle) (25). It will be important to elucidate how these complexes are organized to form the structure for efficient cellulose synthesis.

The amino acid sequences deduced from the *axcesD* genes show a higher degree of conservation than those deduced from other genes in the *axces* operon among cellulose-producing *A. xylinum* family (22), although the homologs of *axcesD* genes are not present in the databank of sequenced plant genes (16). AxCeSD encoded by this gene is not essential for cellulose synthase activity, but cells with disruption of the *axcesD* gene show a marked decrease in BC yield, suggesting that AxCeSD is required for maximal BC synthesis in *A. xylinum* (21). It has been suggested that AxCeSD may play a role in extrusion and/or crystallization of the cellulose sub-elementary fibrils (SEF) (21). However, the detailed function and mechanism of action of AxCeSD in cellulose biosynthesis remain unclear.

In the present study, we obtained the first structure of a bacterial cellulose synthase subunit D, AxCeSD from *A. xylinum*. This subunit, AxCeSD, is assembled into a novel octamer with central pores, which has direct implications for extrusion of the glucan chain into the

extracellular medium. Based on the structure complexed with cellopentaose (CPT, a short glucan chain) and the phenotypes of mutant cells, the current report discusses the function of AxCeSD in extrusion of glucan chains as well as insights into cellulose biosynthesis.

Results

Structure determination and the monomer structure

The crystal structure of AxCeSD with a His_6-tag at the N-terminus (N_AxCeSD) was determined by the multiple wavelength anomalous diffraction (MAD) method (26) (Fig. 1). The asymmetric unit contains eight copies with an average root mean square deviation (RMSD) of 0.5 Å for Cα atoms (Pro8 – Arg150). Based on the N_AxCeSD model, we found that the N-terminus of AxCeSD may be important for its function (*e.g.*, it may influence central pore assembly, as discussed later). Therefore, AxCeSD with a His_6-tag at the C terminus (C_AxCeSD) was also constructed and its structure was solved by the molecular replacement (MR) method (27) at 2.8 Å resolution. The C_AxCeSD crystal contains four copies in an asymmetric unit with an average RMSD of 0.4 Å for Cα atoms (144 residues). Although the N_AxCeSD and C_AxCeSD crystals have different space groups ($P3_2$ and $I4_122$, respectively), the average RMSD for Cα atoms (Pro8 – Arg150) between the two monomer structures is 0.6 Å, and they show very similar conformations. The N- and C-terminal loops (residues 1 – 5 and 151 – 156, respectively) are very flexible; the conformations are different even in copies within the asymmetric unit; residues 1 – 5 could not be built in five of eight copies in N_AxCeSD crystal form; residues 1 – 4 could not be built in three copies, and residues 1 – 3 and 152 – 156 could not be built in remain one of four copies in the C_AxCeSD crystal form. The structure of C_AxCeSD complexed with CPT (C_AxCeSD-CPT) prepared by the crystal soaking method was determined (residues 4 – 151, 4 – 161, 4 – 162, and 4 – 151 in the model) in addition to N_AxCeSD and C_AxCeSD. The full CPT molecules were built and refined based on both 2Fo – Fc and Fo – Fc maps (Fig. 2).

The monomer structure of AxCeSD is composed of five α-helices and four β-strands, with α1 (Thr11 – Val25), α2 (Ile27 – Arg44), α3 (Val53 – Ile67), β1 (Thr71 – Leu77), β2 (Gln81 – Glu88), α4 (Leu104 – Ser118), β3 (Tyr126 – Arg130), α5 (Ala134 – Ala139), and β4 (Ile145 – Val151) ordered from the N-terminus to the C-terminus (Fig. 1a). The four β-strands form an antiparallel sheet (β1 – β2 – β4 – β3), flanked by four α-helices (α1 – α4) on one side and one α-helix (α5) on the other. The arrangement of the two helices (α1 and α2) in the N-terminus resembles a fishhook shape. Interestingly, this structural feature has been found in a very different protein named TRAPP I, a transport protein particle I involved in ER-to-Golgi trafficking. TRAPP I is a multi-subunit vesicle tethering complex composed of seven subunits (PDB: 3CUE) (28, 29). The structure of AxCeSD was shown to be similar to a subunit of TRAPP I by DALI search (30) with a Z score of 10.3 for 127 residues.

Molecular cylinder with four spiral interfaces of dimers

In the crystal structure of N_AxCeSD (space group $P3_2$), an octamer (tetramer of dimers) is formed with a non-crystallographic D_4 point group symmetry in an asymmetric unit (Fig. 1b), which is consistent with the results of gel filtration experiments (Fig. S1). The monomers in each of four dimers are related by the non-crystallographic 2-fold symmetry axes which lie perpendicular to the non-crystallographic axis of 4-fold symmetry of the octamer. This characterization was also confirmed by the crystal structure of the C_AxCeSD (space group $I4_122$), in which although there are only two dimers in an asymmetric unit, an octamer with D_4 point group symmetry is generated by a crystallographic 2-fold axis. Furthermore, small-angle X-ray scattering experiments using N_AxCeSD solution showed a gyration

radius (Rg) of 34.2 Å, corresponding to the calculated Rg value of 34.4 Å from the crystal structure of octamer N_AxCeSD (Fig. S2). These results taken together indicate that AxCeSD exists in an octamer as a functional unit, and the His_6-tag in both of N- and C-terminus do not affect the formation of AxCeSD octamer. We discuss the AxCeSD octamer in this paper.

As shown in Fig. 1a, the two helices α1 and α2 at the N-terminus with a fishhook-like arrangement in two monomers are intertwined and consequently a stable homodimer is assembled with 2-fold symmetry. The monomer contacts in the dimer are mainly made along the faces of these two N-terminal helices and two loops, one linking α3 and β1 and the other connecting β2 and α4, through hydrophobic interactions. In addition, side chain – side chain contacts including Gln15 – Arg44' and Glu20 – Glu36' contribute to dimerization (here, the prime refers to the second monomer in the dimer). Upon dimer formation, an average of approximately 15.5% of accessible surface area on each monomer is buried.

An octameric assembly, a tetramer of dimers AB, CD, EF, and GH, shows a cylindrical structure along the non-crystallographic 4-fold symmetry axis with a height of ~65 Å, an outer diameter of ~90 Å, and an inner cavity diameter of ~25 Å (Fig. 1b). The upper layer of the octamer is comprised of four monomers, A, C, E, and G, while the bottom half consists of the remaining monomers, B, D, F, and H (Fig. 1c). The two layers are twisted by about 50 °. As shown in the side view in Fig. 1b, each monomer interacts with both monomers of the right-side dimer, and only one monomer (same layer) of the left-side dimer. The interactions between monomers of different dimers in the same layer are made mainly by helix α3 and the C-terminal half of the loop bridging α2 – α3 to the right-side monomer in the upper layer,

and by helix α1 and the loop bridging β2 – α4 to the left-side neighbor, while the contact between different layer monomers is formed by C-terminus of α2 and the N-terminal half of the following loop (Figs. 1b and S3). Finally, four dimers are held together in a cylindrical shape with 4-fold symmetry, burying an average of 30% of the accessible surface area in each monomer. Interestingly, the interfaces between dimers form four spiral interstices on the wall of the molecular cylinder with an angle of 50° from the cylinder (vertical) axis (Fig. 1c). All N-termini of the eight AxCeSD molecules extend to the center of the cylinder, while all C-termini are positioned outside on two sides of the cylinder.

Passageway of glucan chain through AxCeSD cylinder

The crystal of C_AxCeSD-CPT complex was prepared by soaking native crystals in crystallization solution with CPT, and its structure was determined by the same method used for determination of the C_AxCeSD structure. Both 2Fo – Fc and Fo – Fc maps showed electron density blobs along the dimer interface in the structure of C_AxCeSD-CPT complex (Fig. 2a), which did not appear in native structures. The electron density blobs were shaped similar to the structure of CPT, and interestingly the center part was bulged, the shape of which corresponds to two β-D-glucopyranoses (Fig. S4). Considering that the 2-fold symmetry axes of AxCeSD dimers are in the centers of blobs, two conformations for each CPT were built close to the inner wall of the molecular cylinder on the dimer interface based on electron density blobs. Two conformations for each CPT located at the same dimer interface are in opposite directions related by either crystallographic or non-crystallographic 2-fold symmetry (Fig. S4c). Finally, based on Fo-Fc map, the eight CPTs with half (0.3) of

total occupancy (0.6) were refined. This means that four CPTs are located in an AxCeSD octamer with two possible orientations each in opposite direction, and the result of refinement corresponds to the average crystal structure of two alternative orientations. Such structural features of C_AxCeSD-CPT complex suggested that AxCeSD does not recognize the direction of CPT as expected from D_4 symmetry of the octamer; it has 2-fold symmetry running through the centroid and perpendicular to the main axis of the cylinder.

As shown in Fig. 2b, the N-termini of the AxCeSD octamer form four passageways together with the inner wall of AxCeSD. Each CPT passes through its own passageway. In accordance with D_4 point group symmetry, the passageways are associated with crystallographic or non-crystallographic 2-fold symmetry running in the same way as dimer assemblage of C_AxCeSD. Half of each passageway is formed by the N-terminus of α1 and the loop prior to α1 (CPT contact residues: Lys6, Asp9, Thr11, Gln15, Gln92) in the first monomer (*i.e.*, monomer A), and the C-terminal half of α3 (CPT contact residues: Ala62', Ala65', and Leu66') in the second monomer (*i.e.*, monomer B) that forms a dimer with the above monomer. Following the symmetry, the other half of the passageway is formed by the C-terminal half of α3 (CPT contact residues: Ala62", Ala65", and Leu66") in the third monomer (*i.e.*, monomer C) that is located at the left side of the first monomer, and the N-terminus of α1 and the loop prior to α1 (CPT contact residues: Lys6"', Asp9"', Thr11"', Gln15"') in the forth monomer (*i.e.*, monomer D) dimerized with the third monomer. Among the CPT contacted residues, the side chains of Lys6, Asp9, and Thr11 were positioned within the hydrogen bonding distance to the CPT.

Compared with the surrounding residues, the CPT was refined with higher average B

factor and lower occupancy, suggesting that the CPTs are flexible with relatively weak interactions of AxCeSD. This flexibility of CPTs can be considered a suitable feature for the motion of glucan chains. The weak affinity between AxCeSD and the glucan chain is important for the extrusion of glucan chains in cellulose production, as discussed below. Taken together, these results indicate that a glucan chain can be extruded through the passageway in the AxCeSD cylinder with no directionality. The extrusion direction of the glucan chain in *A. xylinum* cells may be controlled by other factors. Furthermore, the passageways in the AxCeSD octamer are tilted from the cylinder axis, which may result in the extrusion of glucan chains into the extracellular SEF of cellulose in a right-handed twisted manner (Fig. 2b right).

As described above, the structure of the AxCeSD indicated that the N-terminus was important for cellulose synthesis; therefore, we prepared N-terminus deletion mutants of AxCeSD and measured cellulose productivities of mutant strains to verify their effects on cellulose biosynthesis. In comparison to the cellulose yield of the wild-type strain *A. xylinum* ATCC23769 (100%), the relative yield of the *axcesD* deletion mutant strain DBCD (Fig. S5) was 9.6%, indicating a significant decrease in cellulose yield (Fig. 3a). When the *axcesD* gene was reintroduced into DBCD (DBCD+D), the relative yield of cellulose was recovered to 87.8% of that in controls. With introduction of each plasmid containing the mutant *axcesD* genes in which residues 1-4 (DBCD+DΔN4), 1-5 (DBCD+DΔN5), and 1-6 (DBCD+DΔN6) of AxCeSD were deleted, the relative cellulose yield was less than 30% for DBCD+DΔN6, whereas those of DBCD+DΔN4 and DBCD+DΔN5 were of the same level as that of DBCD+D (Fig. 3a). These results were consistent with the observation that the four

N-terminal residues were disordered in the three structures of AxCeSD, and the inner four passageways of the molecular cylinder were completed from residue Glu5 (Figs. 2b and 3b). As shown in Fig. 3b, the model of DΔN5 (deletion of the five N-terminal residues) retains the inner four passageways, while the passageways are broken in the DΔN6 (deletion of the six N-terminal residues). Based on these results, Lys6 seems to play a critical role in the production of glucan chains by simply creating interior passageways (Fig. 3b) or by forming hydrogen-bonding with the middle glucopyranose ring of CPTs (Fig. 2b)

Discussion

Intramembrane TCs have been suggested to be responsible for the polymerization and extrusion of glucan chains during cellulose synthesis (21, 25, 31). Among the four subunits of the TC, AxCeSA and AxCeSB are known to play roles in glucan chain polymerization and regulation respectively, being capable of binding UDP-Glucose and cyclic-di-GMP (1, 2, 21). AxCeSC and/or AxCeSD were suggested to hold the pore for extruding glucan chains (16, 21, 25, 31, 32). However, it remains unknown how the newly synthesized glucan chains are extruded out of the cell.

The cylinder-shaped structures of N_AxCeSD, C_AxCeSD, and C_AxCeSD-CPT octamer indicate the molecular basis of the passageway for export of glucan chains. The N-terminal loop, especially residue Lys6, plays an important role in glucan chain export, as confirmed by the cellulose production of mutant cells with *axcesD* gene disruption and truncation. The results of the present study suggest that AxCeSD may form an interior cylinder of TC pore, and provides spiral passageways for extruding glucan chains. The weak interaction between

AxCeSD and glucan chains mentioned above would be beneficial for newly synthesized glucan chains to extend through the passageway.

Although the importance of the spiral passageways required confirmation by further studies, it is conceivable that such unique construction of AxCeSD passageways may help spin glucan chains and assemble them together. The SEF would be formed after glucan chains are extruded from the AxCeSD octamer. Considering the physicochemical properties of BC produced by *A.xylinum* and conservation of subunit D in this organism, the AxCeSD octamer may be the key for such unique properties of BC. The effects of AxCeSD on physicochemical properties of cellulose remain to address in further studies.

The complicated processes of BC biosynthesis are performed by TCs present in large quantities in pore sites that are arranged in a linear row in the cell membrane. As of all processes should be closely coordinated, and it is therefore reasonable that TC subunits are well organized. The results of the present study clearly showed that AxCeSD exists as an octamer as a functional unit. Taking into consideration the expression levels of proteins encoded by genes in one operon, the AxCeSD octamer suggests that one TC could be composed of eight sets of subunits A, B, C, and D in *A. xylinum*, and synthesizes and transfers four glucan chains across the membrane through the TC pore. This corresponds to the previous proposal that a glucan chain may be synthesized by two catalytic A-subunits (33, 34). Taking all of these observations together, a model $[(A_2B_2)_4C_8D_8]$ of bacterial TC can be proposed. According to this model, subunits A_2 and B_2 work together to synthesize a glucan chain from the substrate UDP-Glc, and the nascent four glucan chains are then passed through the AxCeSD octamer in the inner TC pore formed by the AxCeSC octamer.

Materials and Methods

The expression, purification, crystallization and data collection of AxCeSD with a His_6-tag (N_AxCeSD, C_AxCeSD) are provided in SI text. The preparation of *axcesD* gene deletion mutant strain (DBCD) is also provided in SI text.

Structure solution and refinement

The X-ray diffraction data were collected using the in-house X-ray diffraction equipment, and the synchrotron radiation. All data sets were processed with the *HKL2000* software suite (35). Se-MAD phasing was applied to solve the N_AxCeSD structure. The sites of selenium atoms were found using the program *SHELXD* (36), and the initial phase was calculated and modified by the program *SHELXE* (36), then a partial structure of 599 residues of polyalanine was constructed with the program *RESOVLE* (37). With this partial structure, the phase was improved iteratively using *OASIS2004* (38), *DM* (39), and *RESOLVE*, and a model of 888 residues was obtained. The additional model building, fitting, and refinement were carried out automatically with the program *LAFIRE* (40) running with the refinement program *CNS* (41) following several cycles of manual model checking and fitting using the graphics program *O* (42). TLS refinement with non-crystallographic symmetry restraint was finally performed using *REFMAC5* (43, 44). The programs *PROCHECK* (45) and *WHATIF* (46) were used to assess the quality of the final model.

The structure of C_AxCeSD was determined by the molecular replacement method with the program *MOLREP* using the dimer structure of N_AxCeSD as a search model, and the structure of C_AxCeSD-CPT was determined by rigid-body refinement using the structure of

C_AxCeSD. While the refinement process of C_AxCeSD was performed as described for that of the N_AxCeSD structure, the refinement of C_AxCeSD-CPT had additional steps for CPT; the CPTs were built based on the Fo – Fc map calculated from the refined protein structure of C_AxCeSD-CPT using the program *COOT* (47). The final refinement of C_AxCeSD-CPT complex with two conformations and total 0.6 occupancy for CPT (Fig. S3) was performed using the program *REFMAC5*. The refinement statistics are listed in Table S1.

Assay of cellulose production

Various *axcesD* genes expressing N-terminus-truncated AxCeSD were amplified by PCR from genomic DNA of *A. xylinum* ATCC23769. Using specific primer pairs corresponding to the predicted 5' and 3' termini (Tab. S2), the PCR products were digested with *Bam*HI/*Hin*dIII, and then cloned into the pTI99 vector. The kanamycin resistance gene was inserted into the *Nde*I site of each plasmid constructed for screening of recombinant strains. The resultant plasmids were introduced into DBCD by electroporation.

A. xylinum was grown in HS medium (48) containing 0.5% (w/v) peptone, 0.5% (w/v) yeast extract, 0.115% (w/v) citric acid, 0.27% (w/v) Na_2HPO_4, and 2% (w/v) D-glucose at 30 °C without shaking for 7 days. Appropriate antibiotics were added as required. The BC membrane formed on the surface of a medium was washed with 1% (w/v) NaOH solution to remove medium and cells for a given time, and then with distilled water until NaOH was removed. The purified BC membrane was air-dried and weighed.

Acknowledgments

We thank Dr. Y. Tanaka and Dr. S. Goda for discussions about the SAXA experiment. We also thank the staff of the Japan Synchrotron Radiation Research Institute (JASRI) for their kind help in SAXA and crystal data collection on beam line BL40B2 and BL41XU at SPring-8. This work was supported by a research grants from the National Project on Protein Structural and Functional Analyses and from Sapporo Bioscience Foundation. This work was partially supported by the Regional Innovation Cluster Program (Global Type).

REFERENCES

1. Saxena IM, Brown RM Jr (2005) Cellulose biosynthesis: current view and evolving concepts. *Ann Bot* 96:9-21.
2. Ross P, Mayer R, Benziman M (1991) Cellulose biosynthesis and function in bacteria. *Microbiol Rev* 55:35-58..
3. Doblin MS, Kurek I, Jacob-Wilk D, Delmer DP (2002) Cellulose biosynthesis in plants: from genes to rosettes. *Plant Cell Physiol* 43:1407-1420.
4. Kimura S, Kondo T (2002) Recent progress in cellulose biosynthesis. *J Plant Res* 115:297-302.
5. Taylor NG (2008) Cellulose biosynthesis and deposition in higher plants. *New Phytol* 178:239-252.
6. Yamanaka S, Watanabe K, Kitamura N, Iguchi M, Mitsuhashi S, Nishi Y, Uryu M (1989) The strucuture and mechanical properties of sheets prepared from bacterial cellulose. *J Mater Sci* 24:3141–3145.
7. Yoshinaga F, Tonouchi N, Watanabe K (1997) Research progress in production of bacterial cellulose by aeration and agitation culture and its application as a new industrial material. *Biosci Biotech Biochem* 61:219-224.
8. Klemm D, Schumann D, Udhardt U, Marsch S (2001) Bacterial synthesized cellulose - artificial blood vessels for microsurgery. *Prog Polym Sci* 26:1561-1603.
9. Nakayama A, et al. (2004) High mechanical strength double-network hydrogel with bacterial cellulose. *Adv Funct Mater* 14:1124-1128.
10. Yano H, et al. (2005) Optically transparent composites reinforced with networks of

bacterial nanofibers. *Adv Mater* 17:153-155.

11. Shah J, Brown RM Jr (2005) Towards electronic paper displays made from microbial cellulose. *Appl Microbiol Biotechnol* 66:352-355.
12. Krystynowicz A, et al. (2002) Factors affecting the yield and properties of bacterial cellulose. *J Indust Microbiol Biotech* 29:189-195.
13. Baklagina YG, et al. (2003) Structural parameters of cellulose produced by *Acetobacter xylinum* and their variation in the course of drying of gel films. *Rus. J Appl Chem* 76: 989-996.
14. Kawano S, et al. (2002) Effects of endogenous endo-beta-1,4-glucanase on cellulose biosynthesis in *Acetobacter xylinum* ATCC23769. *J Biosci Bioeng* 94:275-281.
15. Römling U (2002) Molecular biology of cellulose production in bacteria. *Res Microbiol* 153:205-212.
16. Delmer DP (1999) Cellulose biosynthesis: exciting times for a difficult field of study. *Ann Rev Plant Physiol Plant Mol Biol* 50:245-276.
17. Brown RM Jr, Willison JH, Richardson CL (1976) Cellulose biosynthesis in *Acetobacter xylinum*: visualization of the site of synthesis and direct measurement of the in vivo process. *Proc Natl Acad Sci USA* 73:4565-4569.
18. Itoh T, Kimura S, Brown RM Jr (2004) Theoretical considerations of immunogold labeling of cellulose synthesizing terminal complexes. *Cellulose* 11:385-394
19. Volman G, Ohana P, Benziman M (1995) Biochemistry and molecular biology of cellulose biosynthesis. *Carbohyd Eur* 12:20-27.
20. Wong HC, et al. (1990) Genetic organization of the cellulose synthase operon in

Acetobacter xylinum. *Proc Natl Acad Sci USA* 87:8130-8134.

21. Saxena IM, Kudlicka K, Okuda K, Brown RM Jr. (1994) Characterization of genes in the cellulose-synthesizing operon (acs operon) of *Acetobacter xylinum*: implications for cellulose crystallization. *J Bacteriol* 176:5735-5752.
22. Umeda Y, et al. (1999) Cloning of cellulose synthase genes from *Acetobacter xylinum* JCM 7664: implication of a novel set of cellulose synthase genes. *DNA Res* 6:109-115.
23. Kawano S, et al. (2002) Cloning of cellulose synthesis related genes from *Acetobacter xylinum* ATCC23769 and ATCC53582: comparison of cellulose synthetic ability between strains. *DNA Res* 9:149-156.
24. Benziman M, Haigler CH, Brown RM, White AR, Cooper KM (1980) Cellulose biogenesis: polymerization and crystallization are coupled processes in *Acetobacter xylinum*. *Proc Natl Acad Sci USA* 77:6678-6682.
25. Zaar K (1979) Visualization of pores (export sites) correlated with cellulose production in the envelope of the gram-negative bacterium *Acetobacter xylinum*. *J Cell Biol* 80:773-777.
26. Hendrickson WA (1991) Determination of macromolecular structures from anomalous diffraction of synchrotron radiation. *Science* 254:51-58.
27. Vagin A, Teplyakov A (1997) MOLREP: an automated program for molecular replacement. *J Appl Crystallogr* 30:1022-1025.
28. Cai Y, et al. (2008) The structural basis for activation of the Rab Ypt1p by the TRAPP membrane-tethering complexes. *Cell* 133:1202-1213.
29. Kim YG, et al. (2006) The architecture of the multisubunit TRAPP I complex suggest a

model for vesicle tethering. *Cell* 127:817-830.

30. Holm L, Sander C (1995) Dali: a network tool for protein structure comparison. *Trends Biochem Sci* 20:478-480.

31. Hirai A, Tsuji M, Horri F (2002) TEM study of band-like cellulose assemblies produced by *Acetobacter xylinum* at 4 °C. *Cellulose* 9:105-113.

32. Kimura S, Chen HP, Saxena IM, Brown RM Jr, Itoh T (2001) Localization of c-di-GMP-binding protein with the linear terminal complexes of *Acetobacter xylinum*. *J Bacteriol* 183:5668-5674.

33. Charnock SJ, Davies GJ (1999) Structure of the nucleotide-diphospho-sugar transferase, SpsA from *Bacillus subtilis*, in native and nucleotide-complexed forms. *Biochemistry* 38:6380-6385.

34. Tarbouriech N, Charnock SJ, Davies GJ (2001) Three-dimensional structures of the Mn and Mg dTDP complexes of the family GT-2 glycosyltransferase SpsA: a comparison with related NDP-sugar glycosyltransferases. *J Mol Biol* 314:655-661.

35. Otwinowski Z, Minor W (1997) Processing of X-ray diffraction data collected in oscillation mode. *Methods Enzymol*276:307-326.

36. Sheldrick GM (2008) A short history of SHELX. *Acta Crystallogr* A64:112-122.

37. Terwilliger TC (2003) Automated main-chain model building by template matching and iterative fragment extension. *Acta Crystallogr* D59:38-44..

38. Hao Q, Gu YX, Zheng CD, Fan HF (2000) OASIS: a computer program for breaking phase ambiguity in one-wavelength anomalous scattering or single isomorphous substitution (replacement) data. *J Applied Crystallogr* 33:980-981.

39. Cowtan K (1994) The CCP4 suite: programs for protein crystallography. *Acta Crystallogr* D 50:760-763

40. Yao M, Zhou Y, Tanaka I (2006) LAFIRE: software for automating the refinement process of protein-structure analysis. *Acta Crystallogr* D62:189-196.

41. Brunger AT, et al. (1998) Crystallography & NMR system: a new software suite for macromolecular structure determination. *Acta Crystallogr* D54:905-921.

42. Jones TA, Zou JY, Cowan SW, Kjeldgaard M (1991) Improved methods for building protein models in electron density maps and the location of errors in these models. *Acta Crystallogr* A47:110-119

43. Murshudov G.N, Vagin AA, Dodson EJ (1997) Refinement of Macromolecular Structures by the Maximum-Likelihood Method. *Acta Crystallogr* D5240-255.

44. Winn MD, Isupov MN, Murshudov GN (2001) Use of TLS parameters to model anisotropic displacements in macromolecular refinement. *Acta Crystallogr* D57: 122-133.

45. Laskowski RA, MacArthur M, Moss DS, Thornton JM (1993) PROCHECK: a program to check the stereochemical quality of protein structures. *J Appl Crystallogr* 26:283-291.

46. Vriend G (1990) WHAT IF: a molecular modeling and drug design program. *J Mol Graph* 8:52-56.

47. Emsley P, Cowtan K (2004) Coot: model-building tools for molecular graphics. *Acta Crystallogr* D60:2126-2132.

48. Schramm M, Hestrin S (1954) Factors affecting production of cellulose at the air/liquid interface of a culture of *Acetobacter xylinum*. *J Gen Microbiol* 11:123-129.

FIGURE LEGENDS

Figure 1. Crystal structure of AxCeSD. (a) Ribbon representation of the dimeric structure of AxCeSD. The two monomers are shown in blue and red, respectively. The helices and sheets are labeled, where the prime refers to the second monomer. (b) Overall structure of the AxCeSD octamer. The octamer structure is viewed along the 4-fold axis (top view) and the dyad axis (side view), with each monomer (A – H) shown in a different color. The N- and C-termini of all copies that are positioned in the center and outside of the cylinder are indicated by the circled N and C (same as in Fig. 1a), respectively. (c) A schematic diagram of the octamer assembly based on side view in (b). The octamer is represented by a cylinder, and monomers (A, C, E, G) and (B, D, F, H) are distributed in the top and bottom layers, respectively. The colors of each molecule correspond with those in Fig. 1b. The dimer – dimer interfaces are depicted with sloping rectangles, and indicated by arrows. Figures a – c were prepared with the program PyMOL (DeLano Scientific LLC, http://pymol.sourceforge.net/).

Figure 2. The structure of AxCeSD complexed with CPT. (a) The CPT and its omitted electron density map. The map along the dimer – dimer interface, shown in cyan chickenwire contoured at 2.0 σ, was calculated in the absence of CPT with coefficients Fo – Fc (left). The inner view of the CPT passageway is shown by the protein surface of four monomers (right). (b) Ribbon representation of AxCeSD octamer in complex with CPT (left), and the relocation of four CPTs in the AxCeSD octamer (right). A magnified view of the pore is shown in the rectangular box. The CPTs and the AxCeSD residues involved in contact with CPT are

shown as stick models. Oxygen and carbon atoms in CPT are colored red and yellow, and oxygen, nitrogen, and carbon atoms in AxCeSD are colored red, blue, and gray, respectively

Figure 3. Effects of *axcesD* gene deletion and mutations on the cellulose production. AxCeSDs with N-termini truncated in various lengths were expressed in DBCD of *A. xylinum* ATCC23769. All measurements of cellulose production were carried out under the similar expression level of TC. (a) The relative yields of cellulose produced by wild-type (column WT) and following mutant cells: *axcesD* gene deletion mutant with a control vector (column DBCD), full-length (columns DBCD+D), deletion of the 4 N-terminal residues (column DBCD+DΔN4), deletion of the 5 N-terminal residues (column DBCD+DΔN5), and deletion of the 6 N-terminal residues (column DBCD+DΔN6). The measurements were done 5 times for each sample. (b) Molecular surfaces of C_AxCeSD (WT; the 3 N-terminal residues were disordered), DΔN5 (deletion of the 5 N-terminal residues) and DΔN6 (deletion of the 6 N-terminal residues) octamer. The colors correspond to eight monomers in the same way of Fig 1b and the CPTs are shown as in Figure 2.

Table S1. Data collection statistics

	N_AxCeSD	C_AxCeSD	C_AxCeSD-CPT
Data collection			
Space group	$P3_2$	$I4_122$	$I4_122$
Cell dimensions			
a, *b*, *c* (Å)	77.7, 77.7, 213.9	133.4, 133.4, 217.8	132,9, 132.9, 216.7
α, β, γ (°)	90.0, 90.0, 120.0	90.0, 90.0, 90.0	90.0, 90.0, 90.0
Resolution (Å)		50–2.7 (2.8–2.7)	50–3.0 (3.11–3.0)
R_{sym} ‡ (%)		6.1 (43.2)	8.8 (39.9)
I/σ (*I*)		20.86 (2.39)	18.04 (3.41)
Completeness (%)		99.8 (99.2)	99.9 (99.9)
Redundancy		8.7 (4.8)	10 (9.0)
Refinement			
Resolution (Å)	20-2.5	20–2.8	15–3.0
No. reflections	44637	24424	17658
R/Rfree (%)	18.1/23.8	20.9/27.6	21.4/28.8
No. atoms			
Protein	9535	4784	4828
Ligand	0	0	224
Water	393	261	179
B factor (Å^2)			
Protein	64.5	63.1	49.8
Ligand	-	-	65.5
Water	64.3	73.3	61.5
R. m. s. deviations			
bond length (Å)	0.014	0.017	0.020
bond angle (°)	1.616	1.845	2.229
Ramachandran plot (%)			
most favored regions	91.2	90.8	86.0
additionally allowed regions	8.8	9.2	14.0

Values in parentheses are for the highest resolution shell. The collection statistics of N_AxCeSD have been reported previously (1).

‡ $R_{sym} = \sum_h \sum_j \left| \langle I \rangle_h - I_{hj} \right| / \sum_h \sum_j I_{hj}$, where $\langle I \rangle_h$ is the mean intensity of symmetry-equivalent reflections.

Table S2. Primers and Plasmids

Primers	
sense primers	
SP(C_AxCeSD)	catgccatggcaatttttgagaaaaaaccggatttcaccctgtttc
SP(D_Eco)	cggaattcctgcgtgaggtcggacggggcatgacaatttttgagaaaaaaccggatttcaccc
SP(D_Glu5_Eco)	cggaattcctgcgtgaggtcggacggggcatggagaaaaaaccggatttcaccctgtttc
SP(D_Lys6_Eco)	cggaattcctgcgtgaggtcggacggggcatgaaaaaaccggatttcaccctgtttcttcag
SP(D_Lys7_Eco)	cggaattcctgcgtgaggtcggacggggcatgaaaccggatttcaccctgtttcttcag
SP(Km_Nde)	aaacatatgtgaagaaggtgttgctgactc
R4(C)-bcsxA	tgacaacaccgccccacttcttgc
SP(bcsD)	tcgaattcggacgagccagtaatgacaatttttgag
antisence primers	
AP(C_AxCeSD)	cccaagcttggtcgcggaactgcgcac
AP(D_Hind)	gaaagctttcaggtcgcggaactgcgcacg
AP(Km_Nde)	aaacatatgggaaagccacgttgtgtctc
R2-bglxA	acagagcaacgatcccgccaaac
AP(bcsD)	tcggatcccctgcctcaggtcgcggaactg
Plasmids	
pET-28b	Km^r, P_{T7}, *ori* (pBR322), *lacI*^{q}
pTrc99A	Ap^r, P_{trc}, T_{rrnB}, *ori* (pBR322), *lacI*^{q}
pFF6	endogeneous plasmid from *A. xylinum* IFO3288
pTI99	shuttle vector between *E. coli* and *A. xylinum*, replication gene from FF6 cloned in *Eco*T22I site of pTrc99A
pTIK	pTI99 with Km^r cassette
pTIDK	pTIK with *axcesD* gene
pTIDΔN4K	pTIK with a gene expressing AxCeSD truncated until fourth amino acid
pTIDΔN5K	pTIK with a gene expressing AxCeSD truncated until fifth amino acid
pTIDΔN6K	pTIK with a gene expressing AxCeSD truncated until sixth amino acid

Figure 1

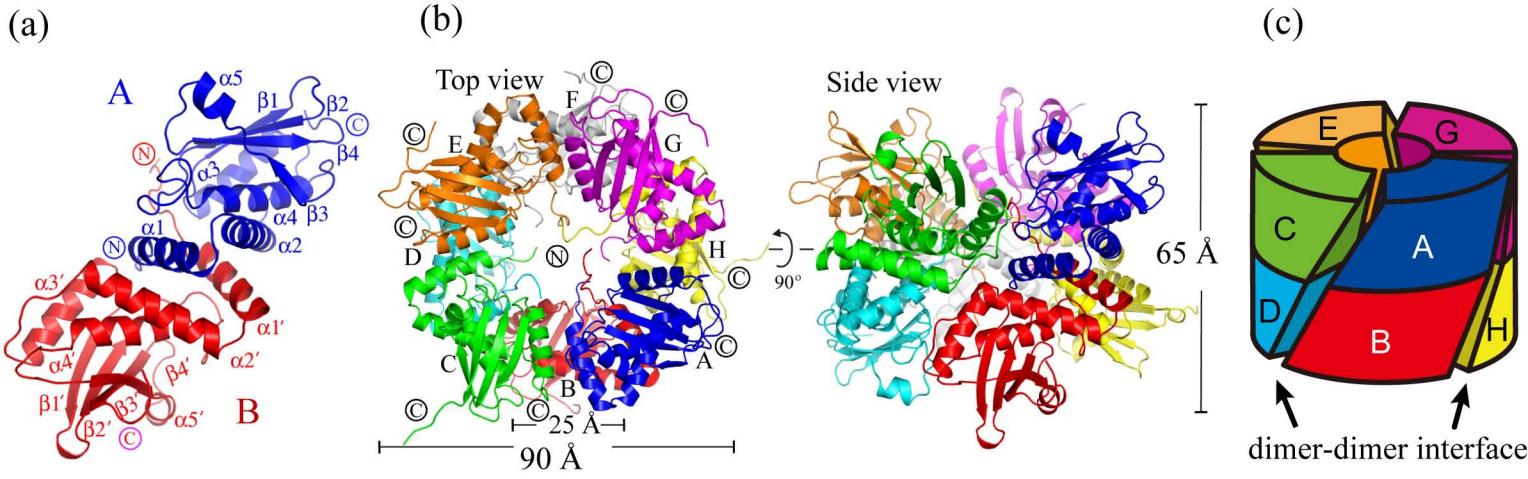
(a)
A
α5
β1
β2
β4
α3
α4
β3
α1
α2
α3′
α1′
α4′
α2′
β4′
β1′
β3′
α5′
β2′
B
(b)
Top view
E
F
G
D
H
C
B
A
25 Å
90 Å
Side view
90°
65 Å
(c)
E
G
C
A
D
B
H
dimer-dimer interface

Figure 2

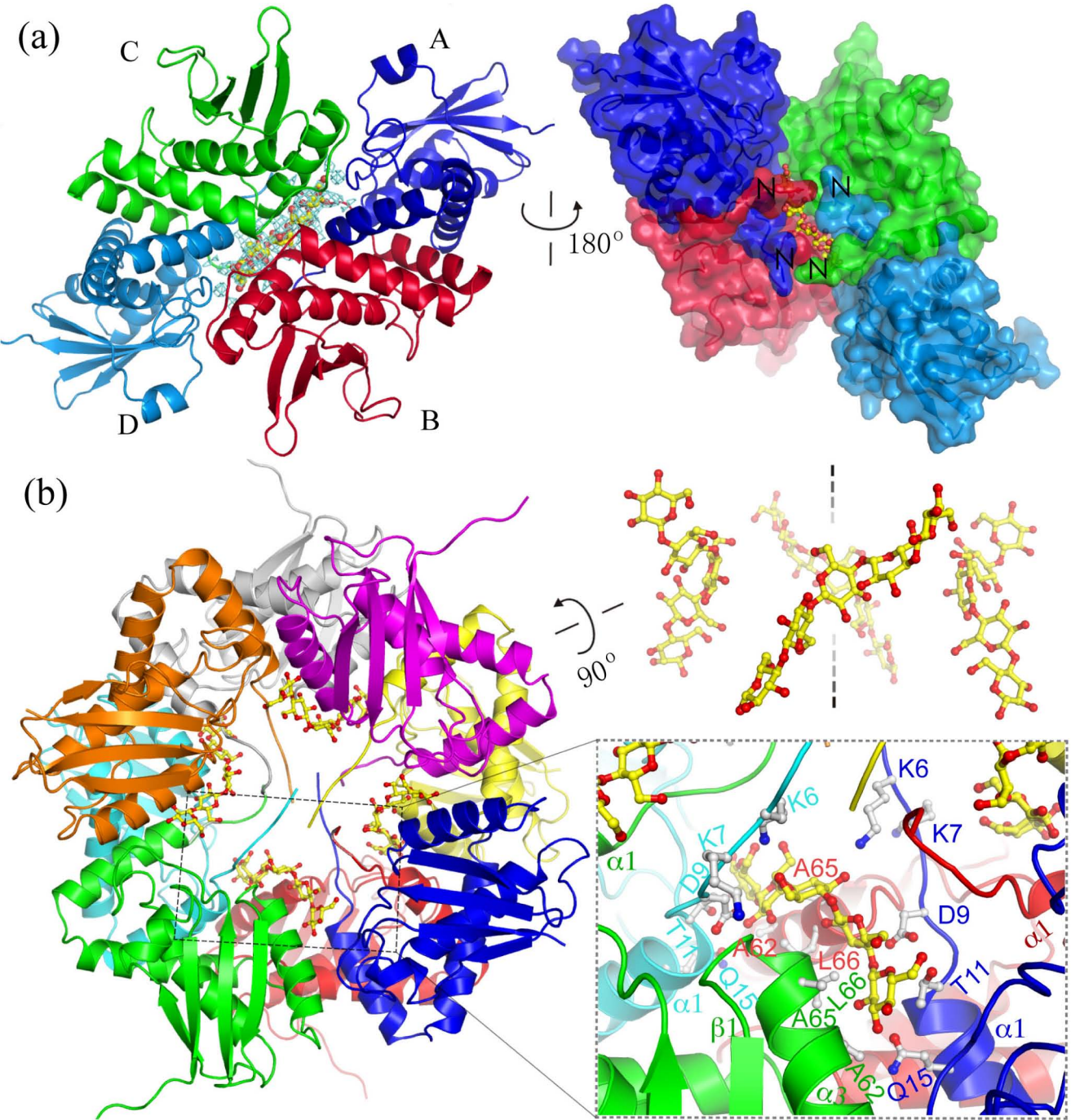
(a)
C
A
D
B
180°
N
N
N
N
(b)
90°
K6
K6
K7
K7
α1
D9
A65
D9
T11
A62
L66
Q15
α1
L66
T11
α1
β1
A65
α1
α3
A62
Q15

Figure 3

(a)

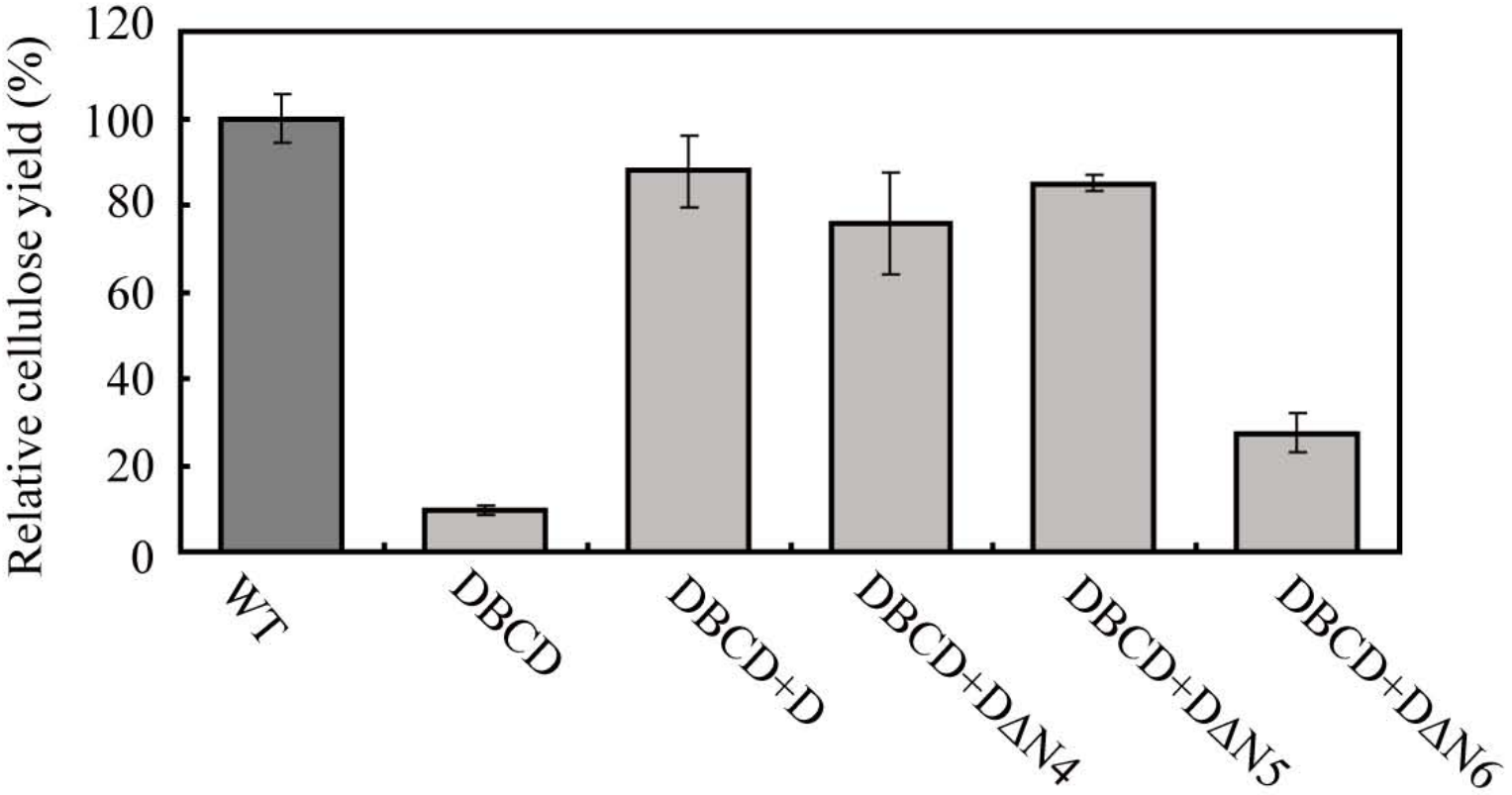
Relative cellulose yield (%)
120
100
80
60
40
20
0
WT
DBCD
DBCD+D
DBCD+DΔN4
DBCD+DΔN5
DBCD+DΔN6

(b)

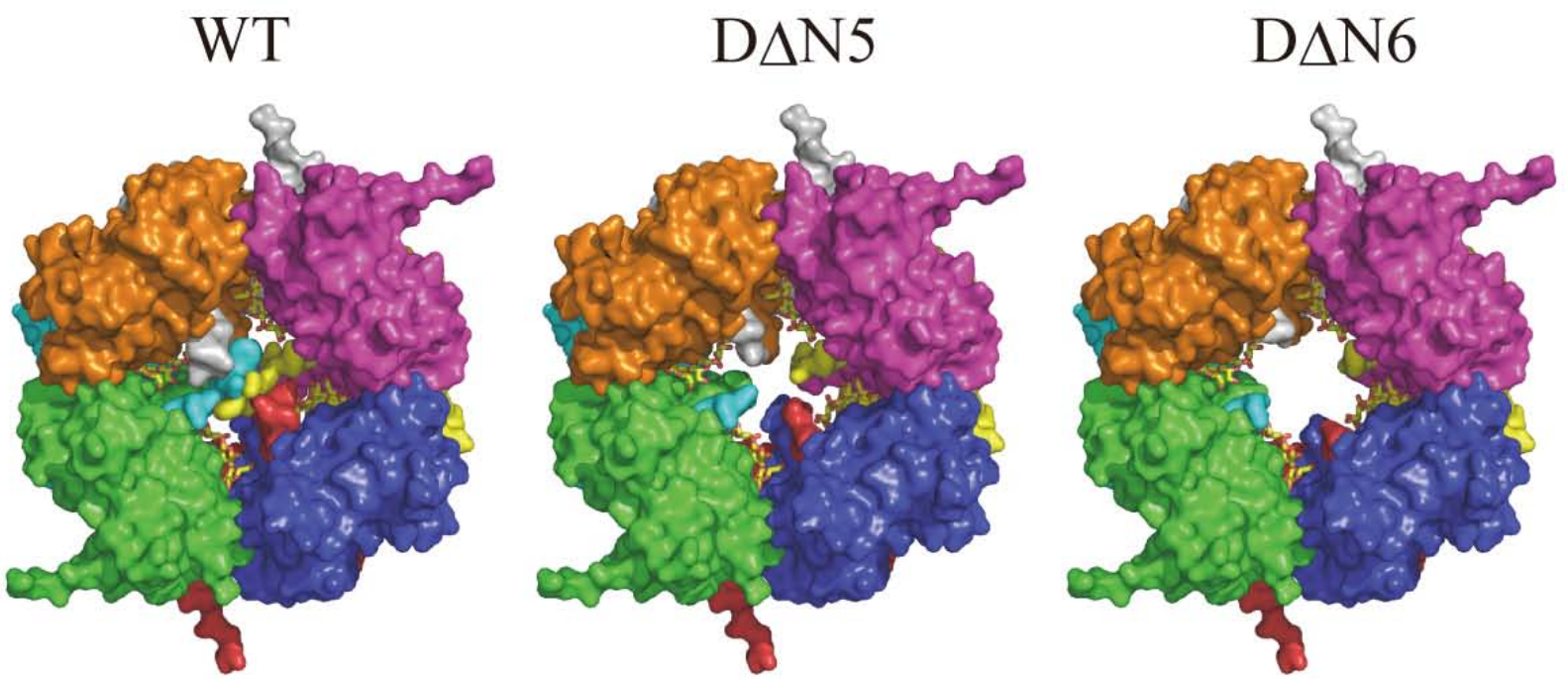
WT
DΔN5
DΔN6